Proceedings of the International Conference on Heat Exchanger Fouling and Cleaning - 2024 (Peer-reviewed)
April 21–26, 2024, Lisbon, Portugal; Editors: H.U. Zettler and E.M. Ishiyama

EXTENSION OF A SIMPLIFIED PHYSICAL FLUSHING PROCESS MODEL TO REALISTIC FLUID PROPERTY VARIATION OF CHOCOLATES

***V. Liebmann[1], M. Heide[2], C. Golla[1], H. Köhler[2], F. Rüdiger[1] and J. Fröhlich[1]**
[1] Institute of Fluid Mechanics, TUD Dresden University of Technology, Germany, vera.liebmann@tu-dresden.de
[2] Institute of Natural Materials Technology, TUD Dresden University of Technology, Germany

ABSTRACT

Experiments and fully resolved numerical simulations are reliable, yet costly ways of designing safe and efficient flushing processes. An alternative is the use of a simplified algebraic model. In this work a model previously developed by the present authors for combinations of fluids with identical properties is extended to different fluid properties of previous and flushing fluid. A realistic range of fluid properties is determined. The results from the simplified model are compared to highly resolved numerical data. The simplified model is able to predict the flushing process well, for phases were only the removal of previous fluid near the wall is relevant. This is achieved quickly, when the previous fluid has a lower apparent viscosity than the displacing one. In the opposite case, the prediction quality of the model for the preceding phase is low and other approaches should be considered.

INTRODUCTION

Flushing processes are used to clean closed equipment used in the production of liquid food products [1]. Due to hygienic risks and industry related restrictions, some products must not be cleaned using aqueous solutions. In the chocolate and lubricant manufacturing, for example, previous product is therefore cleaned from closed equipment using a second flushing product [2, 3]. The flushing process must be designed in such a way, that the product quality of both batches and in the case of chocolate the consumer safety can be ensured by the manufacturer. At the same time, using two valuable products in the flushing process, results in large economic losses, which in the case of lubricant manufacturing exceed one million US dollars per year for a typical large scale facility [3].

Flushing processes can be divided into different phases [4–6]. At the beginning the entire domain, which is usually a pipe or a duct, is filled with previous product and the flushing fluid enters the domain through an inlet. During the first phase, called “core removal”, the previous product at the center of the domain is replaced by the flushing product. The remaining layer of previous fluid on the wall of the domain is removed in the subsequent phase called “layer removal” [6] or “film removal” [4, 5]. Palabiyik et al. [4, 5] identify a third phase, where the very thin film remaining on the wall breaks up and is removed in patches. Depending on the flow conditions and the cleaning system, which consists of the substrate, the previous and flushing fluid [7], the second and third phase may be modelled in numerical simulations using boundary condition cleaning models (BCCM) [8–13]. In the present work, the phases are named in accordance to Liebmann et al. [6].

Flushing processes are influenced by a variety of factors. The rheology of both fluids, their density and miscibility are among the important material properties that affect the flow. Further influencing factors include the geometry, the orientation of the flushed domain and the operating conditions, e.g., the Reynolds number of the flow and temperature.

The removal of various fluids with non-Newtonian behavior, e.g., yoghurt, apple sauce, toothpaste, hand cream, shampoo from a pipe using water as flushing fluid was studied by Palabiyik et al. [4, 5] experimentally. The flow of the flushing fluid was turbulent and a linear relationship between the dimensionless cleaning time and the ratio of the products yield stress and the wall shear stress was found. The dimensionless cleaning time was obtained from the cleaning time using the velocity of the fluid and the pipe diameter. It was also reported, that the prediction of the cleaning time based on dynamic viscosity alone revealed no clear relationship for the wide variety of fluids investigated [5].

Pelipenko et al. [14] investigated the displacement of drilling mud, spacer fluid, wash and cement slurry in a concentric annulus numerically. They developed a mathematical equation to model the movement of the interface of two Herschel-Bulkley fluids in laminar flow. Because the gap of the concentric annulus was very small compared to the radii of the inner and outer cylinder, it was assumed, that the position of the interface at a given time is a function of the azimuthal and axial coordinate only. The resulting model explains the

ISBN: 978-0-9984188-3-4; Published online www.heatexchanger-fouling.com

intuitive understanding of the flow. However, it is only applicable to very thin annular gaps.

Bakhtiyarov et al. [15] investigated the displacement of a Newtonian fluid by a non-Newtonian fluid of the same density inside a horizontal pipe both theoretically and experimentally. A model to determine the time needed for the front to reach a given cross section was developed. This so called breakthrough time is influenced mainly by the viscosity ratio of the involved fluids, the imposed constant pressure gradient, the pipe dimensions and the rheology of the displacing fluid. The model agrees well with experimental data for cases where the viscosity of the previous fluid is smaller than the flushing fluids, but shows up to 20% error for cases, where the viscosities of previous and flushing fluid are reversed.

Allouche et al. [16] investigated the displacement of two non-Newtonian Bingham fluids inside a plane channel numerically. They focused on cases, where the yield stress and the viscosity of the displacing fluid are smaller than those of the displaced fluid. In such cases, static residual layers may arise on the wall, when the yield stress of the previous fluid is not overcome. The authors presented a numerical method based on a transport equation and the continuity equation to describe the flow as well as two-dimensional numerical simulations. The results show that the static residual layers tend to a constant thickness, which depends on the ratio of the yield stresses of both fluids and the equilibrium viscosity of the flushing fluid.

Several researchers used an Arbitrary Lagrangian-Eulerian finite element method to model the displacement of two immiscible Newtonian fluids in a vertical pipe and an annulus [17, 18]. The method is able to predict the interface well near the wall but cannot predict the shape of the front of the displacing fluid near the center of the domain. The use of a dimensionless time to evaluate the breakthrough time was demonstrated in [18]. This scaling is based on the physical time, velocity and length of the section the breakthrough time is determined for.

The displacement of miscible fluids with moderate viscosity ratios in nearly horizontal pipes and ducts was studied by Taghavi et al. [19]. The results indicate that the displacement efficiency is reduced when the viscosity of the previous fluid is larger than that of the flushing fluid.

Liebmann et al. [20] investigated flushing processes of pipework numerically for two non-Newtonian fluids with similar density and a moderate ratio of the two fluids yield stresses. The large viscosity of both fluids resulted in laminar flow at small Reynolds number. A dimensionless time was used, which was calculated from the maximum velocity, the time and the distance of the considered cross-section from the inlet. It was found that the flow was not affected by the elbow bend included in the considered pipework. The use of the dimensionless time allowed for comparison of results in different cross sections. In subsequent work [21], the effect of temperature on the flushing process was studied. A lower apparent viscosity of the previous fluid compared to that of the flushing fluid leads to faster flushing, which can be achieved by heating the previous product or the walls.

Using the same numerical approach, simulations for eight different cases with varying flow velocity, temperature and combination of previous and flushing fluid are validated against experimental data presented by Heide et al. [22]. The numerical results show very good agreement with the experimental data. While the simulation data allowed for detailed insight into the flow features without the need for a test facility, the results took multiple days to be generated.

Since both fully resolved numerical simulations and experiments are costly, they cannot be applied to design flushing processes of entire facilities or large ranges of fluid properties. A computationally inexpensive and quick way to model flushing processes of non-Newtonian fluids in pipes was proposed by Liebmann et al. [6]. The simplified model is based on solving a transport equation for a phase indicator α and assumes identical properties of the previous and flushing fluid. While the full scale numerical simulation of a pipe with length $L = 1$ m requires multiple days of computation time, the simplified model yields accurate results for the considered case within seconds [6]. For large differences in the fluid properties, especially the rheology model parameters, the predictive quality of the simplified model is expected to decrease since the model assumptions are violated. The wide application of the simplified model for cases where the fluid properties vary significantly is therefore currently not possible.

In this contribution the flushing process of two non-Newtonian fluids in a pipe is investigated numerically. As an exemplary process, chocolate flushing is considered, where a previous chocolate is flushed out by second flushing chocolate. A wide range of realistic fluid properties is determined and used in subsequent numerical simulations to investigate their influence on the flushing process. The results are compared to the simplified model introduced by Liebmann et al. [6] to evaluate the models performance for varying fluid properties. Finally, an extension of the simplified model is proposed here and evaluated regarding its capability to predict the numerical results.

DETERMINING REALISTIC FLUID PROPERTY VARIATION OF CHOCOLATES

In both the food and petroleum industry fluids with non-Newtonian rheology occur. This is frequently modeled using the Herschel-Bulkley

ISBN: 978-0-9984188-3-4; Published online www.heatexchanger-fouling.com

model [23], the Bingham model [24], the Casson model and the Windhab model [23, 25]. The latter was first introduced by Eischen and Windhab [26] and uses the following equation for $\tau \geq \tau_0$:

$$\tau = \tau_0 + (\tau_1 - \tau_0)\left(1 - \exp\left(-\frac{\dot{\gamma}}{\dot{\gamma}^*}\right)\right) + \eta_\infty \dot{\gamma} \qquad (1)$$

For $\tau < \tau_0$, the fluid is not yielded and $\dot{\gamma} = 0$. The model contains four parameters with physical meaning, so that it is able to capture more complex rheological behavior. Once the yield stress τ_0 is overcome, a shear-induced loss of structure occurs. At $\dot{\gamma} = \dot{\gamma}^*$ this loss attains its maximum. The parameter τ_1 is referred to as extrapolated yield stress [25]. Finally, the equilibrium viscosity η_∞ is the apparent viscosity reached at high shear rates. Setting $\tau_0 = \tau_1 = 0$ leads to an equation for a Newtonian fluid, whereas setting $\tau_0 = \tau_1 \neq 0$ leads to an equation for a Bingham fluid.

For foodstuff, e.g., chocolate, an excellent fit of the rheological behavior was demonstrated using either the Power-Law, the Casson or the Windhab model by Glicerina et al. [27]. For this contribution chocolate was chosen as exemplary previous and flushing fluid and the Windhab model, see Eq. (1), was chosen as the rheological model. By adapting the model constants, different behavior of both fluids can be represented. In order to determine a realistic range of the fluid properties, the Windhab model parameters were evaluated for six white, seven milk and six dark chocolates. They were determined using the method described in previous works [20, 22]. As an example, τ_0 and τ_1 for all of these samples are depicted in Fig. 1. A linear fit $\tau_1 = 1.58\tau_0$ (coefficient of determination $COD = 0.93$) between both variables is used to reduce the amount of free parameters for the investigation. Furthermore, the yield stress of the chocolates is seen to vary between $\tau_0 = 8$ Pa and 50 Pa. For η_∞ and $\dot{\gamma}^*$ other fits can be found using the same dataset. In this contribution $\eta_\infty/[\text{Pa s}] = 0.14\tau_0/[\text{Pa}]$ and $\dot{\gamma}^*/[\text{s}^{-1}] = 43.8(\tau_0/[\text{Pa}])^{-0.5}$ are used. With these decisions, the yield stress τ_0 becomes the only parameter to describe the rheological behavior. Any such fluid is referred to as a "model fluid" hereafter. To cover the entire range of realistically occurring values of τ_0, six model fluids $\tau_0 = \{5,10,20,30,40,50\}$ Pa are used. It should be noted, that the values reported for the shear rate dependent viscosity of oil at various temperatures by Pedersen et al. [28] fall within the range investigated in the present work. A similar approach could thus be followed to investigate flushing processes in oil manufacturing.

Since most flushing processes include products of similar ingredients, their densities do not vary significantly. For this reason, equal densities for previous and flushing fluid are assumed and set to $\rho = 1000\ \text{kg/m}^3$ here. Both fluids are considered to be immiscible.

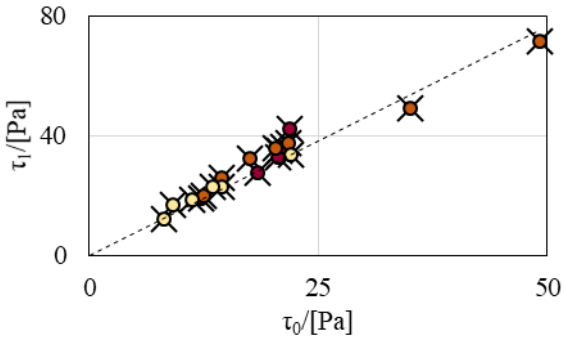

Fig. 1. Windhab model parameters τ_0 and τ_1 of 19 different samples of chocolates and linear fit indicated by the dashed line. Color corresponds to color of chocolate.

SIMULATION IN OPENFOAM

Simulation Setup

The simulations were conducted using the multiphase flow solver multiphaseInterFoam of OpenFOAM v7 which uses the volume of fluid (VOF) method to track the distribution of the respective phases in a multiphase flow. The continuity and momentum equations were solved together with a transport equation for the phase indicator α, which specifies how much flushing fluid is contained in a cell.

Gravitational effects were neglected, as they were shown to have no significant influence forn the flow regime considered here [20]. Hence, the flow is expected to be axisymmetric and the computational domain was reduced to a wedge of the pipe with axisymmetric boundary conditions in azimuthal direction. This greatly reduces the computational cost. The domain consists of a linearly extruded wedge with an opening angle of $\beta = 2°$ and a side length of $R = D/2$ where $D = 0.05$ m is the diameter of pipe. The inlet is located at $x = 0$ and the outlet at $x = L = 10\,D$. A total of 50 cells was used to resolve the radial direction with an increased resolution near the wall, where cell smallest has a height of $\Delta r/R = 0.009$. In azimuthal and axial direction one cell and 200 cells were employed respectively. This results in a total of 10 k cells for one simulation.

At the inlet, flushing fluid enters the domain. The velocity profile of fully developed axial pipe flow of flushing fluid was imposed, with an average velocity of $u_\text{b} = 0.1$ m/s. The domain is initially filled with previous fluid. Its velocity distribution corresponds to the analytical solution of developed flow of previous fluid inside a pipe. The analytical solution for developed pipe flow of a single Windhab fluid can be found in the literature and consists of a fully yielded region towards the wall and an unyielded region towards the pipe center

ISBN: 978-0-9984188-3-4; Published online www.heatexchanger-fouling.com

[29]. In the unyielded region a constant maximum velocity u_{max} occurs which stretches from the pipe center at $r = 0$ to the plug flow radius $r_0 = 2\tau_0/f$, where f is the absolute value of the pressure gradient.

The rheological data of both fluids is based on the parameters determined in the previous section. The rheological model, see Eq. (1), was implemented in OpenFOAM and limited to a maximum viscosity of $\nu_{max} = 10^4\eta_\infty/\rho$ for numerical reasons, as previously discussed in the literature [20].

A total of 25 simulations were carried out using different values of m. Here, $m = \tau_{0,F}/\tau_{0,P}$ refers to the ratio of the yield stresses of the flushing fluid and previous fluid. Both previous and flushing fluid were chosen from the model fluids described in the second section. Combinations of these fluids were chosen to cover a large range of m. For simulations with $m < 1$, the yield stress of the flushing fluid is listed in Table 1. The cases with $m > 1$ were simulated as well, with the yield stress of the flushing fluid and previous fluid being interchanged. An additional simulation was carried out for $m = 1$ and $\tau_{0,F} = 20$ Pa.

Table 1. List of simulations with $m < 1$.

m	[−]	0.1	0.13	0.17	0.2	0.25	0.33
$\tau_{0,F}$	[Pa]	5	5	5	10	10	10
m	[−]	0.4	0.5	0.6	0.67	0.75	0.8
$\tau_{0,F}$	[Pa]	20	10	30	20	30	40

Simulation results

Evaluation procedure. To quantify the height of the remaining layer, the radial position of the interface of the two fluids was determined, termed the contact radius r_c here. With the VOF method, the interface cannot be tracked explicitly, so that its position was identified with the position where $\alpha = 0.5$, which was obtained by interpolation.

Interface progression for different yield stress ratios m. The progression of the interface of the two fluids throughout the domain over time is shown in Fig. 2 for the case where $m = 2.5$. The interface progresses quickly, with constant velocity, in the center of the pipe. As a result, the center is completely filled with flushing fluid after a little more than three seconds. This is due to the flushing fluid progressing with u_{max} for $0 \leq r \leq r_{0,F}$. With increasing radial position, the interface progresses over shorter axial distances, since the velocity $u(r)$ decreases towards the wall.

Fig. 3 displays a comparison of the interface shape for different ratios $m > 1$ at the same physical time $t = 2.5$ s and in Fig. 4 for $m < 1$. In all cases shown in Fig. 3, a common flushing fluid with $\tau_{0,F} = 50$ Pa and thus the same inlet velocity profile

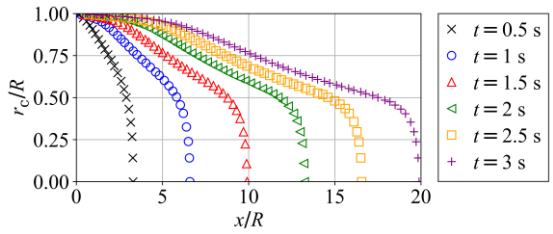

Fig. 2. Contact radius r_c along the pipe axis at different times for $\tau_{0,F} = 50$ Pa and $m = 2.5$.

was used, whereas in Fig. 4 the same previous fluid $\tau_{0,P} = 50$ Pa was chosen. For comparison the analytical solution for $m = 1$ is shown in both figures.

Three regions can be distinguished in the graph for all cases. Near the wall the contact radius is an almost linear function of the axial position, while in the center of the pipe the axial position is constant over the radius. In between these two, an intermediate region is observed, featuring one turning point of the profile for $m < 1$ and two turning points for $m > 1$, while the profile has none for $m = 1$.

With decreasing difference between $\tau_{0,F}$ and $\tau_{0,P}$, the numerical results are increasingly closer to the analytical solution for $m = 1$, which is expected. For $m > 1$, both the yield stress $\tau_{0,F}$, the equilibrium viscosity $\eta_{\infty,F}$ and thus the apparent viscosity of the flushing fluid are greater than that of the previous fluid. This leads to an increased displacement in axial direction for fully yielded regions $r \gg r_0$ and thus the slope near the wall tends to a nearly horizontal position. Near the center of the pipe, where the apparent viscosity tends to ν_{max}, this

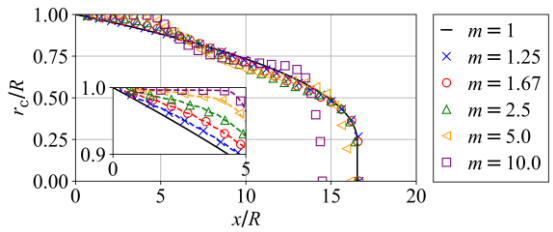

Fig. 3. Contact radius r_c over axial coordinate x at $t = 2.5$ s from the numerical simulations for selected ratios $m > 1$, all with $\tau_{0,F} = 50$ Pa and analytical solution for $m = 1$.

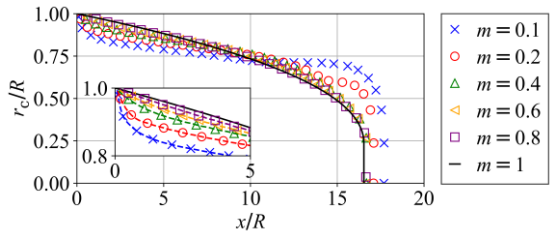

Fig. 4. Contact radius r_c over axial coordinate x at $t = 2.5$ s from the numerical simulations for selected ratios $m < 1$, all with and $\tau_{0,P} = 50$ Pa and analytical solution for $m = 1$.

ISBN: 978-0-9984188-3-4; Published online www.heatexchanger-fouling.com

displacement is inhibited and to fulfill continuity the interface progresses shorter distances in axial direction for $m > 1$. While for moderate ratios $1 \leq m \leq 2.5$, the difference between the cases is almost not perceptible the deformation of the interface near the wall can clearly be seen for larger m.

For $m < 1$ the opposite effect is observed. The interface progresses further in axial direction towards the pipe center with decreasing m, i.e., with increasing difference between $\tau_{0,\mathrm{F}}$ and $\tau_{0,\mathrm{P}}$. This can be observed by the increasing absolute value of the slope near the wall. Within the transition region, the slope tends to an almost constant value, which can be seen best for the lowest ratios m. This means, that between the flushing front at large x and the inlet at $x = 0$, the contact radius tends to an almost constant value over x with decreasing m. For moderate ratios $m > 0.4$ the difference between the cases is relatively small compared to those at high ratios.

Evolution of the interface when rescaling time. For most industrial flushing processes, a relevant question to help determine the end of the flushing process is the time needed to obtain a target value for the contact radius, as this gives insights into contamination risks. This can be visualized by plotting either the contact radius over time $r_\mathrm{c}(t)$ for a discrete location x or by plotting the contact radius over the axial coordinate $r_\mathrm{c}(x)$ at a discrete time t as shown in Fig. 3 and Fig. 4.

Both approaches may be combined by using a non-dimensional time $\hat{t} = t u_{\max}/x$. Here, $u_{\max}$ is the velocity of the flushing fluid within the unyielded region of the flushing fluid. This representation has several advantages, as $r_\mathrm{c}(\hat{t})$ leads to a comprehensive visualization of how much flushing time needs to pass to obtain the targeted contact radius. Since $\hat{t}^{-1} = x/(u_{\max} t) = \hat{x}$ could be interpreted as dimensionless distance, plotting the contact radius over the inverse of the dimensionless time, i.e., $\hat{t}^{-1}$, offers a dimensionless representation of the position of the interface.

With increasing time, the interface stretches in axial direction. When $m = 1$, where no radial velocity components occur. By using the dimensionless representation this manifests itself as a common graph of the dimensionless interface and of the contact radius over dimensionless time. Any deviation from the common graph is due to radial velocity components and a resulting deformation in that direction, which occurs, whenever $m \neq 1$.

Fig. 5 shows plots of the contact radius over dimensionless time for $m = 2.5$, $m = 1$ and $m = 0.4$ exemplarily. For $m = 1$ it can easily be seen that all curves form a common graph. At $\hat{t} = 1$ the core removal phase begins with a steep increase of r_c/R over dimensionless time. Once the slope of r_c/R decreases, the core removal phase transitions into the layer removal phase. Qualitatively, the graphs

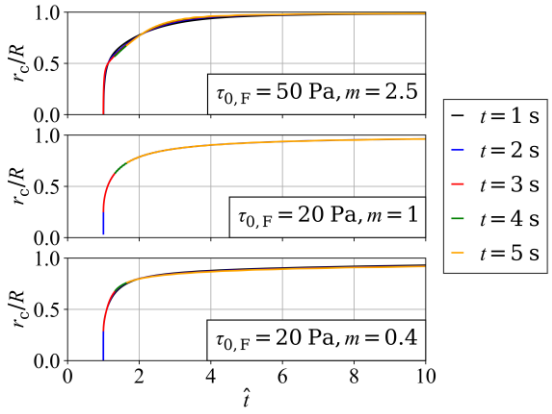

Fig. 5. Interface over dimensionless time for three different cases.

looks similar for the two cases where $m \neq 1$ in Fig. 5. However, it can be seen, that slight deviations occur over time.

For small dimensionless times, i.e., during the core removal phase, this deformation is most prominent. With increasing physical time, the graphs converge to a constant shape. For $m = 2.5$ the interface moves further towards the wall at $r/R = 1$, whereas for $m = 0.4$, the interface deforms away from the wall. Comparing the three cases, different contact radii are achieved in the same dimensionless time.

The results for different ratios m and the dimensionless time needed to obtain four different exemplary target values of r_c are plotted in Fig. 6. With increasing m and decreasing target value of r_c, the dimensionless time needed to reach that value decreases. For some low values of m, e.g., $m = 0.1$, none of the target values were obtained within the simulation time. Therefore, no data is shown for those ratios. Fig. 6 shows, that the dimensionless time needed to obtain a target value of r_c decreases non-linearly with increasing m. This is in line with the observation of the deformation of the interface with changing m. It should be noted, that the results form a common graph for each target contact radius, even though the yield stress of the flushing fluid $\tau_{0,\mathrm{F}}$ is varied between the simulations. For the investigated bulk velocity u_b, the ratio of the two yield stresses m, therefore is the main influence on the flushing time. Furthermore, the layer removal phase, which is crucial in determining the end of a flushing process, can be visualized at different locations and times using the dimensionless time.

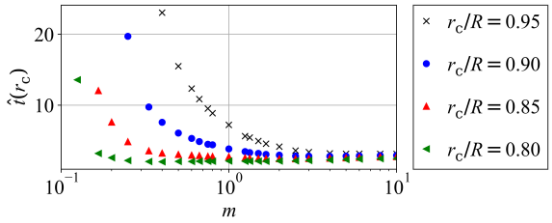

Fig. 6. Dimensionless time needed to obtain different contact radii for varying m.

ISBN: 978-0-9984188-3-4; Published online www.heatexchanger-fouling.com

EXTENSION OF SIMPLIFIED MODEL

Model overview

The results of the previous section illustrate that for $m \approx 1$ the solution obtained with $m = 1$ provides a reasonable approximation for the flushing process, but for larger values an improvement of the approach is needed. The model previously developed by the authors is based on solving the transport equation for the phase indicator α with $m = 1$ [6].

$$\partial_t \alpha + u_{\mathrm{tr}} \partial_x \alpha = 0 \tag{2}$$

Here, u_{tr} corresponds to a transport velocity in axial direction for the phase indicator α. For the special case $m = 1$, the properties of previous and flushing fluid are identical. Therefore, u_{tr} can be set to the solution of a single phase inside the pipe and contact radius for both core and layer removal can be determined analytically. For $m \neq 1$ the transport velocity depends on the fluid present at a given radius. This is accounted for by using the analytical solution of two phase annular flow $u(r)$ as transport velocity, which will be derived in the following section. Since the location of r_{c} is a priori unknown $u_{\mathrm{tr}} = u(r = r_{\mathrm{c}})$ is chosen.

Analytical solution of axisymmetric flow of two Windhab fluids

Steady axisymmetric and developed flow of two Windhab fluids with a common density inside a pipe is considered. The absolute value of the pressure gradient in axial direction f is assumed to be constant and no other external forces influence the flow. The streamwise momentum equation in cylindrical coordinates yields

$$f = \frac{1}{r} \frac{\partial (r \tau_{rx})}{\partial r} \tag{3}$$

This holds for the flushing fluid and the previous fluid, denoted by using the index $i = \mathrm{F}$ and $i = \mathrm{P}$, respectively. Integrating Eq. (3) over the radius r and applying the symmetry condition at $r = 0$ gives

$$\tau_i = \tau_{rx} = f \frac{r}{2} \tag{4}$$

which holds for both phases. Hence, the shear stress is a linear function of the pressure gradient in axial direction. Inserting the Windhab model, see Eq. (1), for regions where $\tau_i \geq \tau_{0,i}$, i.e., where $r \geq r_{0,i}$, leads to

$$u_{\mathrm{i}}(r) = \omega_{\mathrm{i}}(r) + I_{1,\mathrm{i}} \tag{5}$$

$$\omega_i(r) = -\frac{b_i^2}{c_i} \Omega_i(r) - \frac{b_i^2}{2c_i} \Omega_i^2(r) + c_i \frac{r^2}{2} + d_i r \tag{6}$$

$$\Omega_i(r) = W_0 \left(\frac{a_i}{b_i} \exp\left(\frac{d_i + c_i r}{b_i} \right) \right) \tag{7}$$

Here, W_0 is the principal branch of the Lambert W-function which provides the solution $W_0(x) = y$ for equations of type $y e^y = x$. The auxiliary function ω_i and Ω_i contain the rheological parameters a_i, b_i, c_i and d_i of the flushing and previous fluid respectively for $i = \mathrm{F}, \mathrm{P}$. They are determined from $a_i = (\tau_{1,i} - \tau_{0,i})/\eta_{\infty,i}$, $b_i = \dot{\gamma}_i^*$, $c_i = -f/(2\eta_{\infty,i})$, $d_i = \tau_{1,i}/\eta_{\infty,i}$ and depend solely on the rheological properties of the respective fluid, as well as f.

For regions, where $\tau_i < \tau_{0.i}$, i.e., $r < r_{0,i}$, one obtains

$$u_{\mathrm{i}}'(r) = 0 \tag{8}$$

which after integration yields

$$u_i(r) = I_{2,i} \tag{9}$$

The two constants $I_{1,i}$ and $I_{2,i}$ can be determined from the boundary conditions. At the interface both fluid must have the same velocity $u_{\mathrm{P}}(r_{\mathrm{c}}) = u_{\mathrm{F}}(r_{\mathrm{c}})$ and at the wall no slip occurs, i.e., $u_{\mathrm{P}}(R) = 0$. Furthermore, at the plug flow radii the velocity must be continuous.

The parameter space of the problem is quite large, as it is spanned by the plug flow radii of the two considered Windhab fluids $r_{0,\mathrm{i}}$, the pipe radius R, and the contact radius r_{c}. This results in 24 different configurations. Of these, 14 configurations result in single phase flow or no flow, i.e., $u(r) = 0$, because either the contact radius or both plug flow radii are larger than the pipe radius, i.e., $r_{\mathrm{c}} > R$ or $(r_{0,\mathrm{F}} > R) \wedge (r_{0,\mathrm{P}} > R)$. The case $r_{\mathrm{c}} < r_{0,\mathrm{F}} < R < r_{0,\mathrm{P}}$ is also discarded, as it results in no flow. The remaining nine configurations can be clustered into five groups, shown in Fig. 7. The corresponding analytical solution can be determined for each group and is shown exemplarily for the first group, shown on the left in Fig. 7. For this configuration, the contact radius is the smallest of the four radii and the plug flow radius of the previous fluid lies within the pipe, i.e., $(r_{\mathrm{c}} < r_{0,\mathrm{P}}) \wedge (r_{\mathrm{c}} < r_{0,\mathrm{F}}) \wedge (r_{0,\mathrm{P}} < R)$.Below the contact radius unyielded flushing fluid flows at the same velocity as the unyielded previous fluid around it. For $r \geq r_{0,\mathrm{P}}$ the previous fluid is yielded. This leads to

$$u(r) = \begin{cases} \omega_{\mathrm{P}}(r) - \omega_{\mathrm{P}}(R), & r \geq r_{0,\mathrm{P}} \\ \omega_{\mathrm{P}}(r_{0,\mathrm{P}}) - \omega_{\mathrm{P}}(R), & r < r_{0,\mathrm{P}} \end{cases} \tag{10}$$

For the remaining groups shown in Fig. 7, the analytical solution is detailed in the appendix.

For a given pressure gradient the solution for $u(r)$ can be calculated explicitly using the Eq. (10) or the ones given in the appendix. For a given bulk velocity u_{b} the solution has to be determined

ISBN: 978-0-9984188-3-4; Published online www.heatexchanger-fouling.com

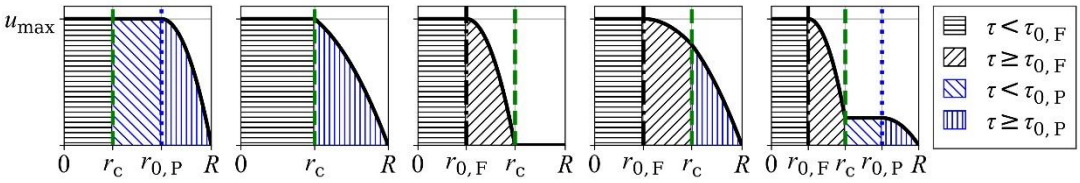

Fig. 7. Schematic representation of the five different configurations of annular flow of two Windhab fluids in a pipe with radius R, depending on the location of the plug flow radii $r_{0,F}$ and $r_{0,P}$ and the contact radius r_c. The yielded and unyielded regions of previous and flushing fluid are distinguishable by different hatchings.

iteratively. The resulting solution is valid for any two fluids with Windhab rheology as long as the assumptions made for the derivation are met. For differing densities of flushing and previous fluid slight modifications have to be made. Since the product densities from one product family typically do not differ significantly the solution might still lead to accurate results. The assumption of a constant layer thickness throughout the pipe is valid during the layer removal phase. The derived solution is therefore expected to lead to accurate predictions of the velocity distribution during this phase. For the core removal phase the assumption of a constant pressure gradient along the pipe axis and a constant pressure within a cross section does not hold. Hence, the model is not applicable to that phase. This is not detrimental, since the duration of the core removal phase is short compared to the duration of the layer removal phase.

Evaluation of the simplified model

In this section, the results of the model using the analytical solution for single phase flow (SPM) [6] and the one using the solution for two phase flow (TPM) as transport velocity u_{tr} are shown and compared to the solution obtained using the numerical simulation. Results for three exemplary cases are shown in Fig. 8.

For $m = 2.5$ the contact radius r_c determined using the TPM is in agreement with the numerical simulation for $\hat{t} > 4$. This region mostly belongs to the layer removal phase. During the core removal phase, for $\hat{t} < 4$, the predicted contact radius is larger than the one obtained from the numerical simulation. During that phase, the assumption of a constant layer height, which was made to derive the analytical solution, does not hold. The SPM appears to obtain a better result. This, however, is most likely due to the fact, that in this case, the interface is assumed to not deform at all. Since for $m > 1$ no static residual layers will arise, it can be shown mathematically, that $\lim_{\hat{t}\to\infty} r_c/R = 1$ for both the TPM and the SPM. The difference between both models will therefore tend to zero.

For $m = 1$ both models produce the same results and are in agreement with the fully resolved simulation. This case also serves as mutual validation of both the numerical simulation and the newly derived TPM. For the case, where $m = 0.4$, the numerical data is not predicted well using the TPM during either the core or layer removal phase. In the numerical simulation for $m = 0.4$ the slope of the contact radius tends towards a low value more quickly than in the case where $m = 2.5$, indicating a short core removal phase and quick transition to layer removal in comparison. The TPM consistently predicts lower values for r_c/R and a larger slope, indicating that the core removal phase in this model transitions into the layer removal phase much slower than in the simulations. The assumption of a constant layer thickness, results in no radial velocity components in the TPM. The TPM can therefore only advect the interface in axial direction at a relatively low velocity due to the high viscosity of the previous layer. This leads to a delayed prediction of the cleaned radius. The SPM in comparison obtains better agreement with the simulation data, because it overestimates the velocity at the contact radius.

A feature that makes the TPM superior to the SPM is the ability to predict potential static residual layers of previous fluid on the wall, see Fig. 7 in the middle. For given rheological parameters and bulk velocity u_b the analytical solution can be evaluated, so that $r_{0,P} \geq R$. Of the investigated cases, all those where $m < 0.25$ resulted in a static residual layer.

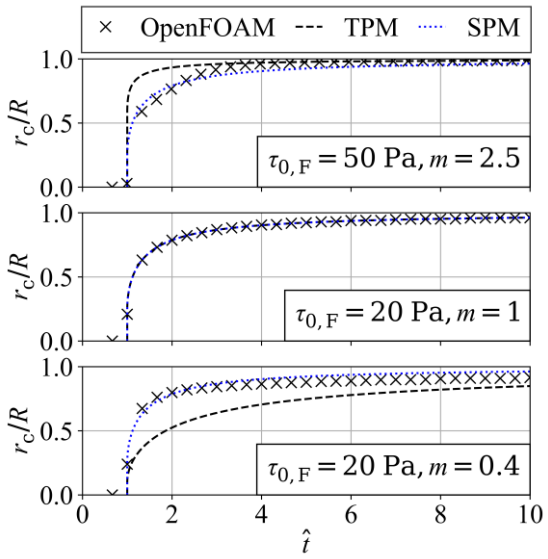

Fig. 8. Contact radius over dimensionless time for three exemplary cases obtained with the data from the numerical simulation (OpenFOAM), the simplified model using the two phase velocity profiles (TPM) and the model from [6](SPM).

ISBN: 978-0-9984188-3-4; Published online www.heatexchanger-fouling.com

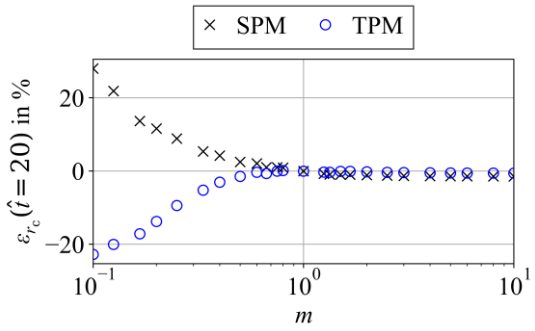

Fig. 9. Ratio of the contact radius obtained with the TPM and SPM respectively and the numerical simulation for different ratios m.

The error for the contact radius obtained with each model is compared to the one in the OpenFOAM simulation $\varepsilon = (r_{\mathrm{c,mod}} - r_{\mathrm{c,OF}})/r_{\mathrm{c,OF}}$ and plotted for all cases at $\hat{t} = 20$. The results are shown in Fig. 9. For $m > 1$, the error is slightly smaller using the TPM. This is due to the assumption of equal properties in the SPM, which for $m > 1$, leads to a higher viscosity compared to the one used in the TPM and thus slower transport of fluid within the remaining previous layer. For $m < 1$, the SPM and TPM obtain increasingly larger absolute errors with decreasing m. The TPM obtains slightly smaller absolute errors than the SPM for $m > 0.5$. For $m < 1$, the SPM overestimates the contact radius and the TPM underestimates the contact radius. In combination both models can be used to determine a corridor, within which the contact radius will be. In addition, only the TPM can predict arising static residual layers.

CONCLUSION

In this contribution flushing processes of non-Newtonian fluids, whose rheology is described by the Windhab model were investigated. Flushing of one chocolate by another was chosen as an exemplary process. Fluids with yield stresses ranging from $\tau_0 = 5 - 50$ Pa were investigated. The range resulted from the analysis of 19 different chocolate samples. Literature data [28] suggests, that various oils at different temperatures could be modeled using a similar range. Thus, the conclusions drawn here can be expanded to oil flushing processes.

A total of 25 numerical simulations were performed to determine the influence of differing fluid properties on the flow. A dimensionless representation of time was used to track the evolution of the contact radius at a given location and to obtain the shape of the interface.

The numerical simulations show that with increasing m the contact radius obtained after the same flushing time increases. For the considered cases, the contact radius depends only on the ratio m and not on the absolute yield stress of either model fluid. The common bulk velocity u_{b} used in this work allows an easy comparison of the material costs. For cases where $m < 1$, significantly more flushing time is necessary to obtain the same contact radius than in cases where $m > 1$.

Using the understanding from the numerical simulations an extension for a simplified algebraic model was proposed to predict the contact radius during both the core and layer removal phase. Therefore, the analytical solution of annular flow of two Windhab fluids was derived, which is not available in the literature to the best of the authors knowledge. The analytical solution is particularly valuable, since the Windhab model captures several other rheological models for special parameter selections, e.g., the Bingham model. Furthermore, the use of the analytical solution allows the prediction of static residual layers, which can arise, when $m < 0.25$ for the investigated bulk velocity of $u_{\mathrm{b}} = 0.1$ m/s.

The results of the TPM and those of the numerical simulations are compared to those of a previously developed model [6]. While the present model outperforms the previous model for $m > 1$ during the layer removal phase, it underestimates the contact radius in the core removal phase. This is due to the neglect of the radial velocity component. The SPM in comparison shows better agreement during the core removal phase. For $m < 1$, both models show significant weaknesses, as the contact radius is over- and underpredicted by almost 20% for the SPM and TPM respectively. Improvement of the present model could be achieved by including the radial velocity component in the model. This, however, would yield a system of partial differential equations, that has to be solved numerically, resulting in larger computational times. The model presented here, can produce results within seconds. For $m > 1$, the TPM can thus be used to obtain quick predictions for flushing processes. For $m < 1$, the combination of the TPM and SPM yield reliable upper and lower bounds for the evolution of the contact radius over time.

The analytical solution of annular flow further allows the quick determination of possible static residual layers. If they occur, the combination of flushing and previous fluid should be avoided, as the complete removal of previous product is not achievable for this combination. Even if no static residual layers arise, the flushing time and material and energy costs are high for cases with low m. For practical applications, it is therefore convenient to use moderate ratios of $m \approx 1$ for cases when $m < 1$. In those cases, the TPM can predict the contact radius with small errors, but at significantly lower computational times, than numerical simulations or experiments.

ISBN: 978-0-9984188-3-4; Published online www.heatexchanger-fouling.com

APPENDIX

Analytical solution for annular two phase flow

Second group $\boldsymbol{r_{0,P} < r_c < r_{0,F}}$**.** The second group, see Fig. 7 second to left, consists only of configurations, where the contact radius is greater than the previous fluids plug flow radius, but smaller, than the flushing fluids plug flow radius. Thus, a yielded region of previous fluid stretches from the wall to the contact radius, where it meets an unyielded flushing fluid. We obtain

$$u(r) = \begin{cases} \omega_\mathrm{P}(r) - \omega_\mathrm{P}(R), & r \geq r_\mathrm{c} \\ \omega_\mathrm{P}(r_\mathrm{c}) - \omega_\mathrm{P}(R), & r < r_\mathrm{c} \end{cases}$$

Third group $\boldsymbol{r_{0,F} < r_c \leq R \leq r_{0,P}}$**.** The third group of configurations, see Fig. 7 in the middle, consists of three regions as well. The previous fluid remains unyielded, i.e., at rest on the wall as a static residual layer. For the flushing fluid a yielded and unyielded region exist.

$$u(r) = \begin{cases} 0, & r \geq r_\mathrm{c} \\ \omega_\mathrm{F}(r) - \omega_\mathrm{F}(r_\mathrm{c}), & r_\mathrm{c} > r \geq r_{0,\mathrm{F}} \\ \omega_\mathrm{F}(r_{0,\mathrm{F}}) - \omega_\mathrm{F}(r_\mathrm{c}), & r_{0,\mathrm{F}} > r \end{cases}$$

Fourth group $\boldsymbol{(r_{0,P} < r_c) \wedge (r_{0,F} < r_c)}$**.** The fourth group, see Fig. 7 second to right, covers configurations, where both plug flow radii are smaller than the contact radius. It consists of three regions. Near the wall, the previous fluid is yielded. At the contact radius, yielded flushing fluid is present, which becomes unyielded towards the pipe center. We obtain $u(r) =$

$$\begin{cases} \omega_\mathrm{P}(r) - \omega_\mathrm{P}(R), & r \geq r_\mathrm{c} \\ \omega_\mathrm{F}(r) - \omega_\mathrm{F}(r_\mathrm{c}) + \omega_\mathrm{P}(r_\mathrm{c}) - \omega_\mathrm{P}(R), & r_\mathrm{c} > r \geq r_{0,\mathrm{F}} \\ \omega_\mathrm{F}(r_{0,\mathrm{F}}) - \omega_\mathrm{F}(r_\mathrm{c}) + \omega_\mathrm{P}(r_\mathrm{c}) - \omega_\mathrm{P}(R), & r_{0,\mathrm{F}} > r \end{cases}$$

Fifth group $\boldsymbol{r_{0,F} < r_c < r_{0,P} < R}$**.** The fifth group, see Fig. 7 on the right, contains yielded and unyielded regions for both fluids and thus consists of four regions. It follows, that $u(r) =$

$$\begin{cases} \omega_\mathrm{P}(r) - \omega_\mathrm{P}(R), & r \geq r_{0,\mathrm{P}} \\ \omega_\mathrm{P}(r_{0,\mathrm{P}}) - \omega_\mathrm{P}(R), & r_{0,\mathrm{P}} > r \geq r_\mathrm{c} \\ \omega_\mathrm{F}(r) - \omega_\mathrm{F}(r_\mathrm{c}) + \omega_\mathrm{P}(r_{0,\mathrm{P}}) - \omega_\mathrm{P}(R), & r_\mathrm{c} > r \geq r_{0,\mathrm{F}} \\ \omega_\mathrm{F}(r_{0,\mathrm{F}}) - \omega_\mathrm{F}(r_\mathrm{c}) + \omega_\mathrm{P}(r_{0,\mathrm{P}}) - \omega_\mathrm{P}(R) & r_{0,\mathrm{F}} > r \end{cases}$$

ACKNOWLEDGMENTS

This research project is supported by the Industrievereinigung für Lebensmitteltechnologie und Verpackung e.V. (IVLV), the Arbeitsgemeinschaft industrieller Forschungsvereinigungen, Otto von Guericke‘ e.V. (AiF) and the Federal Ministry of Economic Affairs and Climate Action (AiF Project IGF 20672 BR).

NOMENCLATURE

Latin symbols

a	Windhab flow solution parameter, $1/\mathrm{s}$
b	Windhab flow solution parameter, $1/\mathrm{s}$
c	Windhab flow solution parameter, $1/(\mathrm{m\ s})$
d	Windhab flow solution parameter, $1/\mathrm{s}$
D	Pipe diameter, m
f	Pressure gradient, $\mathrm{Pa/m}$
I	Integration constant, -
L	Pipe length, m
R	Pipe radius, m
r	Radial coordinate, m
t	Time, s
$\hat{t}$	Dimensionless time, -
W_0	Principal branch of Lambert W function, -
u	Velocity, $\mathrm{m/s}$
x	Axial coordinate, m

Greek symbols

α	Phase indicator used in VOF method, -
β	Opening angle of wedge, °
$\dot{\gamma}$	Shear rate, $1/\mathrm{s}$
$\dot{\gamma}^*$	Windhab-model parameter, $1/\mathrm{s}$
ε	Error, -
η_∞	Windhab-model parameter, Pa s
ρ	Density, $\mathrm{kg/m^3}$
τ	Stress, Pa
τ_0	Yield stress, Pa
τ_1	Windhab-model parameter, Pa
ω	Windhab solution function, $\mathrm{m/s}$
Ω	Windhab solution function, -

Subscript and superscript

b	Bulk
c	Contact
i	Index for flushing and previous phase
F	Flushing
max	Maximum
P	Previous
0	Yield
1,2	Subscripts for constants

REFERENCES

[1] Moerman, F., in *Food Protection and Security*, ed. S. Kennedy, pp. 167-266, Elsevier, Amsterdam, 2017.

[2] Bean, D. C., and Post, L. S., in *The Microbiological Safety of Low Water Activity Foods and Spices*, eds. J.B. Gurtler et al., pp. 269-293, Springer New York, New York, 2014.

[3] Jerpoth, S. S., Hesketh, R., Slater, C. S., Savelski, M. J., and Yenkie, K. M., Strategic Optimization of the Flushing Operations in Lubricant Manufacturing and Packaging Facilities, *ACS Omega*, vol. 8, pp. 38288–38300, 2023.

[4] Palabiyik, I., Olunloyo, B., Fryer, P. J., and Robbins, P. T., Flow regimes in the

ISBN: 978-0-9984188-3-4; Published online www.heatexchanger-fouling.com

emptying of pipes filled with a Herschel–Bulkley fluid, *Chemical Engineering Research and Design*, vol. 92, pp. 2201–2212, 2014.
[5] Palabiyik, I., Lopez-Quiroga, E., Robbins, P. T., Goode, K. R., and Fryer, P. J., Removal of yield-stress fluids from pipework using water, *AIChE Journal*, vol. 64, pp. 1517–1527, 2018.
[6] Liebmann, V., Heide, M., Köhler, H., Golla, C., Fröhlich, J., and Rüdiger, F., Reduced cleaning model for highly viscous non-Newtonian fluids in pipelines, *Computer Aided Chemical Engineering*, vol. 52, pp. 325–330, 2023.
[7] Köhler, H., Liebmann, V., Joppa, M., Fröhlich, J., Majschak, J.-P., and Rüdiger, F., On the Concept of Computational Fluid Dynamics-Based Prediction of Cleaning for Film-Like Soils, *Heat Transfer Engineering*, vol. 43, pp. 1406–1415, 2022.
[8] Joppa, M., Köhler, H., Rüdiger, F., Majschak, J.-P., and Fröhlich, J., Experiments and Simulations on the Cleaning of a Swellable Soil in Plane Channel Flow, *Heat Transfer Engineering*, vol. 38, pp. 786–795, 2017.
[9] Golla, C., Köhler, H., Fröhlich, J., and Rüdiger, F., Numerical modeling of a cohesively separating soil layer in consideration of locally varying soil distribution, *Heat and Mass Transfer*, 2023.
[10] Köhler, H., Liebmann, V., Golla, C., Fröhlich, J., and Rüdiger, F., Modeling and CFD-simulation of cleaning process for adhesively detaching film-like soils with respect to industrial application, *Food and Bioproducts Processing*, vol. 129, pp. 157–167, 2021.
[11] Golla, C., Köhler, H., Liebmann, V., Fröhlich, J., and Rüdiger, F., CFD-based three-dimensional modeling of an adhesively detaching soil layer in a channel flow with sudden expansion, *Food and Bioproducts Processing*, vol. 136, pp. 176–183, 2022.
[12] Golla, C., Jena, S., Liebmann, V., Fröhlich, J., Rüdiger, F., and Köhler, H., Numerical investigation of model soils using a combined cleaning model for film-like soils, *Proceedings of 14th International Conference on Heat Exchanger Fouling and Cleaning 2024*, Lisbon, Portugal 2024.
[13] Golla, C., Liebmann, V., Rebel, R., Köhler, H., Fröhlich, J., and Rüdiger, F., Numerical model for the cleaning of a film-like soil by viscous shifting under non-isothermal conditions, *Proceedings of 14th International Conference on Heat Exchanger Fouling and Cleaning 2024*, Lisbon, Portugal 2024.
[14] Pelipenko, S., and Frigaard, I. A., Mud removal and cement placement during primary cementing of an oil well – Part 2; steady-state displacements, *Journal of Engineering Mathematics*, vol. 48, pp. 1–26, 2004.
[15] Bakhtiyarov, S., and Siginer, D. A., Fluid displacement in a horizontal tube, *Journal of Non-Newtonian Fluid Mechanics*, vol. 65, pp. 1–15, 1996.
[16] Allouche, M., Frigaard, I. A., and Sona, G., Static wall layers in the displacement of two visco-plastic fluids in a plane channel, *Journal of Fluid Mechanics*, vol. 424, pp. 243–277, 2000.
[17] Rasmussen, H. K., Hassager, O., and Saasen, A., Viscous flow with large fluid-fluid interface displacement, *International Journal for Numerical Methods in Fluids*, vol. 28, pp. 859–881, 1998.
[18] Szabo, P., and Hassager, O., Displacement of one Newtonian fluid by another: Density effects in axial annular flow, *International Journal of Multiphase Flow*, vol. 23, pp. 113–129, 1997.
[19] Taghavi, S. M., Alba, K., and Frigaard, I. A., Buoyant miscible displacement flows at moderate viscosity ratios and low Atwood numbers in near-horizontal ducts, *Chemical Engineering Science*, vol. 69, pp. 404–418, 2012.
[20] Liebmann, V., Heide, M., Schoppmann, K., Köhler, H., and Rüdiger, F., Aspects of modelling the cleaning of a chocolate with yield stress in a pipe using CFD, *Fouling and Cleaning in Food Processing Conference 2022*, Lille, France 2022.
[21] Liebmann, V., Heide, M., Köhler, H., Rüdiger, F., and Fröhlich, J., Improving flushing processes through targeted control of the temperature boundary conditions, *PAMM*, vol. 23, pp. e202300253, Dresden, Germany 2023.
[22] Heide, M., Liebmann, V., Rüdiger, F., Majschak, J.-P., and Köhler, H., Experimental studies of the flushing of chocolate masses on a test facility, *Proceedings of 14th International Conference on Heat Exchanger Fouling and Cleaning 2024*, Lisbon, Portugal 2024.
[23] *Handbook of Farm, Dairy and Food Machinery Engineering*, Elsevier, 2013.
[24] Frigaard, I. A., Paso, K. G., and De Souza Mendes, P. R., Bingham's model in the oil and gas industry, *Rheologica Acta*, vol. 56, pp. 259–282, 2017.
[25] Figura, L. O., and Teixeira, A. A., *Food Physics*, Springer Berlin Heidelberg, 2007.

ISBN: 978-0-9984188-3-4; Published online www.heatexchanger-fouling.com

[26] Eischen, J.-C., and Windhab, E. J., Viscosity of Cocoa and Chocolate Products, *Applied Rheology*, vol. 12, pp. 32–34, 2002.

[27] Glicerina, V., Balestra, F., Dalla Rosa, M., and Romani, S., Microstructural and rheological characteristics of dark, milk and white chocolate: A comparative study, *Journal of Food Engineering*, vol. 169, pp. 165–171, 2016.

[28] Pedersen, K. S., and Rønningsen, H. P., Effect of Precipitated Wax on ViscosityA Model for Predicting Non-Newtonian Viscosity of Crude Oils, *Energy & Fuels*, vol. 14, pp. 43–51, 2000.

[29] Pitsillou, R., Georgiou, G. C., and Huilgol, R. R., On the use of the Lambert function in solving non-Newtonian flow problems, *Physics of Fluids*, vol. 32, pp. 093101, 2020.

ISBN: 978-0-9984188-3-4; Published online www.heatexchanger-fouling.com